

# THERMODYNAMIC BEHAVIOR OF $\text{Ca}_3\text{Co}_{3.93+x}\text{O}_{9+\delta}$ CERAMICS

#O. JANKOVSKY, D. SEDMIDUBSKY, Z. SOFER, P. SIMEK, J. HEJTMANEK\*

*Institute of Chemical Technology Prague, Technická 5, Prague, Czech Republic*

*\*Institute of Physics, ASCR, v.v.i., Curkvarnicka 10, Prague, Czech Republic*

E-mail: Ondrej.Jankovsky@vscht.cz

Submitted February 28, 2012; accepted May 11, 2012

**Keywords:** Misfit cobaltites, Thermoelectric materials, Heat capacity, Thermodynamic properties, Debye-Einstein model, Phase equilibria

*Based on the results of differential thermal analysis, differential scanning calorimetry, thermogravimetric analysis, low temperature calorimetry and X-Ray powder diffraction of equilibrated samples as well as on the assessed thermodynamic data phase a section of the Ca–Co–O diagram for  $p_{\text{O}_2} = 0.21$  was calculated using the FactSage software. Among the involved phases the misfit cobaltite  $\text{Ca}_3\text{Co}_{3.93+x}\text{O}_{9+\delta}$  is well known for its distinctive thermoelectric properties. As shown by our experiments and reproduced by the proposed thermodynamic model the  $\text{Ca}_3\text{Co}_{3.93+x}\text{O}_{9+\delta}$  phase actually exhibits a narrow homogeneity range with respect to cation composition. The primary focus was put on the heat capacity of  $\text{Ca}_3\text{Co}_{3.93}\text{O}_{9+\delta}$  collected in a broad temperature range and analyzed in terms of a combined Debye - Einstein model. This made it possible to separate two peaks detected at  $\sim 400$  K and  $\sim 840$  K and to evaluate the corresponding entropy and enthalpy changes. The second effect was interpreted as a spin transition from intermediate state to high state.*

## INTRODUCTION

Thermoelectric energy recovery from waste heat is a promising technology suitable for direct electric power generation. Electric power is generated as a consequence of a thermal gradient between two ends of a conductor thanks to the Seebeck effect. The misfit layer cobaltites have recently attracted a considerable attention in the search for new thermoelectric materials which can be applied in thermoelectric conversion devices operated at elevated temperatures. A typical representative is the  $\text{Ca}_3\text{Co}_{3.93+x}\text{O}_{9+\delta}$  phase. Its structure is composed of  $[\text{CoO}_2]$  blocks and rock-salt type  $[\text{Ca}_2\text{CoO}_3]$  blocks. These building blocks share the overall monoclinic symmetry as well as the corresponding lattice parameters  $a$ ,  $c$  and  $\beta$ , however, they differ in the  $b$  parameters whose ratio  $b_1/b_2 \sim 1.618$  gives rise to the incommensurate character of the structure. The system can be thus described as  $[\text{Ca}_2\text{CoO}_3]^{\text{RS}}[\text{CoO}_2]_{1.62}$  which results in the net formula  $\text{Ca}_3\text{Co}_{3.93}\text{O}_{9.36}$ . Moreover, the structure can accommodate a large deviation from the ideal crystallographic oxygen stoichiometry established as a consequence of oxygen vacancies formation in the  $[\text{Ca}_2\text{CoO}_3]$  block. Consequently the average Co valence in  $[\text{CoO}_2]$  blocks varies in the range 3.2-3.4, while Co in the central layer of  $[\text{Ca}_2\text{CoO}_3]$  blocks is found very close to (but below) the trivalent state. The electric transport is predominantly established in  $[\text{CoO}_2]$  layers built from edge-shared octahedra ( $\text{CdI}_2$  structure pattern) with  $\text{Co}^{\text{III}}$

in low spin state. The holes formed as a result of partial oxidation of  $[\text{CoO}_2]$  layers (formally expressed as  $\text{Co}^{\text{IV}}$ ) are doped into an originally completely filled  $a_{1g}$  band (originating for  $t_{2g}$  band split due to trigonal distortion of the octahedral environment) which is the reason for the positive thermoelectric power [1-2]. The large magnitude of thermopower ( $+160$ - $180$   $\text{mV}\cdot\text{K}^{-1}$ ) is believed to result from an interplay of spin and orbital degrees of freedom together with large slope of density of states at Fermi level and giving rise to large entropy per carrier. Hence thermopower (also referred to as Seebeck coefficient) is largely predetermined by the electronic structure and character of charge carriers and thus can be considered as an intrinsic thermodynamic property of a given material (no matter of the specific form, i.e. whether single crystal or ceramics). However, it can be modified by tuning Fermi level by solid solutions forming and, in the particular case of transition metal oxides, by changing the spin and orbital degree of freedom of itinerant charge carriers. A lot of studies have been performed to examine the influence of various homovalent and heterovalent substitutions or chemical dopant additions [3-6]. If we confine our scope only to Ca–Co–O system itself, there are possibilities how to modify the doping level: the variation of oxygen and cation stoichiometry. The oxygen stoichiometry as a function of temperature and partial pressure of oxygen ( $p_{\text{O}_2}$ ) has been experimentally studied by Shimoyama et al [7] and recently theoretically described by Sedmidubsky et al. [8]. In this work we draw

our attention to the detailed experimental determination of the miscibility range  $x$  in  $\text{Ca}_3\text{Co}_{3.93+x}\text{O}_{9+\delta}$ , which has been also included into the thermodynamic model described in detail in [8].

The experimentalist's effort all over the world is aimed to produce materials with a figure of merit  $ZT$  close to or even higher than unity. To achieve this goal the material must simultaneously exhibit high Seebeck coefficient (thermopower), low electrical resistivity and low thermal conductivity. Compared to Seebeck coefficient, electrical resistivity and thermal conductivity of misfit cobaltites are predominantly influenced by the material microstructure and in particular by the density of matter. To reach a density approaching the theoretical value it is advantageous to use hot pressing technique, which is a method also used for diamond manufacturing. Another method is spark plasma sintering. These methods were discussed in Kenfaui's work [9]. Moreover the prepared materials should be stable and resistant. The second objective of this study is thus to examine the thermal stability of  $\text{Ca}_3\text{Co}_{3.93+x}\text{O}_{9+\delta}$  by means of both the experimental and thermodynamic modeling approach. As the heat capacity as a function of temperature belongs, along with the enthalpy of formation, to key thermodynamic characteristics determining the equilibrium behavior, the emphasis is put on the measurement of  $C_p(T)$  in a broad temperature range using two different techniques and on the detailed analysis of the obtained data.

## EXPERIMENT AND CALCULATIONS

Samples with different Ca/Co ratio were prepared by ceramic route using a solid state reaction. The compositions of samples used for the DTA/DSC tests were  $\text{Ca}_7\text{Co}_3\text{O}_y$  ( $x_{\text{Co}} = 0.3$ ),  $\text{Ca}_3\text{Co}_2\text{O}_y$  ( $x_{\text{Co}} = 0.4$ ),  $\text{CaCoO}_y$  ( $x_{\text{Co}} = 0.5$ ),  $\text{Ca}_3\text{Co}_{3.93}\text{O}_y$  ( $x_{\text{Co}} = 0.57$ ),  $\text{Ca}_1\text{Co}_2\text{O}_y$  ( $x_{\text{Co}} = 0.66$ ) a  $\text{Ca}_1\text{Co}_4\text{O}_y$  ( $x_{\text{Co}} = 0.8$ ). Samples for the determination of the solid state solubility in  $\text{Ca}_3\text{Co}_{3.93+x}\text{O}_{9+\delta}$  were  $x = -0.33, -0.23, -0.13, -0.03, +0.07, +0.17$  and  $+0.27$ . Starting powders of  $\text{CaCO}_3$  and  $\text{Co}_2\text{O}_3$  were mixed and homogenized, calcined in the platinum crucible at 1120 K and 1170 K for 24 hours each and milled in the epicyclic mill *Retsch PM 100* for 40 minutes, milling speed was set at 400 rpm. After milling powders were pressed under pressure of 0.5 GPa. Next step was sintering in oxygen atmosphere ( $p_{\text{O}_2}/p^0 = 1$ , where  $p^0 = 101.3$  kPa) at 1213 K for 100 hours. High partial pressures of oxygen turned out to accelerate the formation of  $\text{Ca}_3\text{Co}_{3.93+x}\text{O}_{9+\delta}$ . Samples were analyzed by Scanning Electron Microscopy (SEM) on *HITACHI S-4700* and *TESCAN Vega 3 LMU*.

All samples were analyzed by X-Ray powder Diffraction (XRD) on *PANalytical X'Pert PRO* diffractometer in Bragg-Brentano parafocusing geometry using  $\text{CuK}_\alpha$  radiation. Data evaluation was performed by means

of the *HighScore Plus* software package and by *KSoft (KDif module)* To confirm the composition of the various parts of the phase diagram at elevated temperatures, a number of high-temperature annealing experiments was performed followed by rapid quenching to room temperature. The sample was pulled from the furnace and thrown into a container with liquid nitrogen. We can assume that all phase transformations to low temperature equilibrium state are kinetically hindered during this short time, so the sample remained in its high temperature thermodynamic equilibrium during the XRPD measurements. During the annealing experiments temperature did not exceed 1300 K.

The low temperature heat capacity of the  $\text{Ca}_3\text{Co}_{3.93}\text{O}_{9+\delta}$  was measured on the *Physical Properties Measurement System (PPMS)* on the equipment *14 T-type* (Quantum Design, USA) using two relaxation time methods under high vacuum in this work in the temperature range 0-298 K. The sample was a compressed powder plate of ~50 mg and densities over 70% of theoretical density. The samples were mounted to the calorimeter platform with cryogenic grease Apiezon N (supplied by Quantum Design). However, prior to the main run with the sample, a blank sample holder with the Apiezon only was measured to obtain background data. The sample heat capacity was then obtained as a difference between the two data sets. This procedure was applied, because the heat capacity of Apiezon is not negligible in comparison with the sample heat capacity (~8 % at room temperature) and exhibits a sol-gel transition below room temperature [10].

Thermal analysis tests were performed by Differential Scanning Calorimetry (DSC) on *Netzsch DSC 404 C Pegasus* calorimeter in the dynamic oxygen and air atmosphere at a heating rate  $10 \text{ K}\cdot\text{min}^{-1}$  within the temperature range 293 K to 1200 K. The measured temperature was calibrated on the melting points of pure metal standards and the apparatus sensitivity was obtained as a function of temperature by measuring the sapphire standard (NIST, ref. N°720) under the same experimental conditions. The heat capacity was calculated from three measurements of the sample (S), blank (BL) and reference (R) as:

$$C_p = \frac{(\phi_S - \phi_{BL}) \cdot M_S}{r \cdot m_S \cdot S} \quad (1)$$

where

$$S = \frac{(\phi_S - \phi_{BL}) \cdot M_R}{r \cdot m_R \cdot C_p} \quad (2)$$

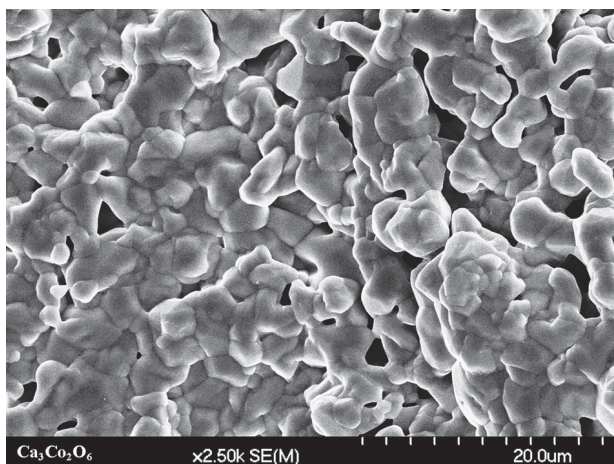
is the sensitivity,  $r$  is the applied heating rate,  $\Phi_i$  are the respective measured signals and  $m_i$  and  $M_i$  the corresponding masses and molar masses.

Differential Thermal Analysis (DTA) and Thermogravimetric Analysis (TG) were used for higher temperature range to confirm phase decompositions at temperatures from 293 K to 1300 K. DTA and TG were

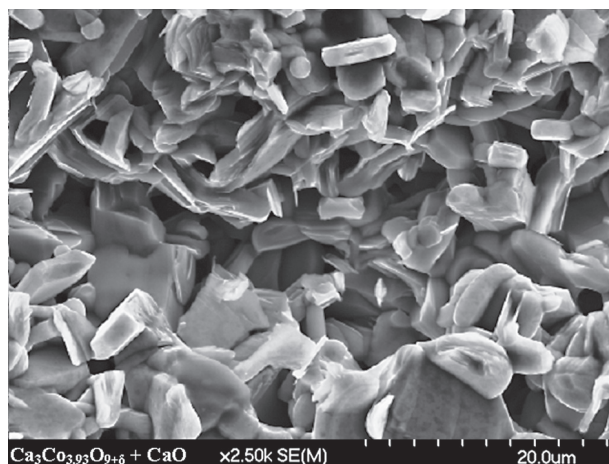
measured simultaneously on *Setaram STA* aperture model *Setsys Evolution* with a heating rate  $10 \text{ K}\cdot\text{min}^{-1}$ . The remaining thermodynamic data required for FactSage calculations were adopted from the data reported in works [8], Hardy et al. [11], Jung et al. [12], Hejtmanek et al. [13], Jakob et al. [14], Woermann et al. [15] and Chen et al. [16]. All data were implemented into FactSage program and the section of the phase diagram for  $p_{\text{O}_2}/p^0 = 0.21$  ( $p^0 = 101.3 \text{ kPa}$ ) was constructed, where  $x_{\text{Co}}$  is between 0.3 and 0.8 in the temperature region to 1300 K.

## RESULTS AND DISCUSSION

Results of XRD analysis of samples with different composition revealed the presence of four phases at laboratory temperatures: rock-salt solid solution  $\text{Ca}_{1-x}\text{Co}_x\text{O}$ ,  $\text{Co}_3\text{O}_4$ ,  $\text{Ca}_3\text{Co}_2\text{O}_6$  and  $\text{Ca}_3\text{Co}_{3.93+x}\text{O}_{9+\delta}$ . However, our FactSage calculations (see the phase diagram in Figure 3) indicate that the  $\text{Ca}_3\text{Co}_2\text{O}_6$  phase should not be stable at low temperatures due to a lower oxygen content compared to the competing  $\text{Ca}_3\text{Co}_{3.93+x}\text{O}_{9+\delta}$ -CaO mixture with the same cation composition. This represents the main difference between our model and up to now the only published Ca-Co-O phase diagram reported by Woermann and Muan [15]. The fact that Woermann and Muan did not observe this decomposition may be ascribed to kinetic effects. Indeed the relatively fast cooling of our sample ( $x_{\text{Co}} = 0.4$ ) after sintering ( $5 \text{ K}\cdot\text{min}^{-1}$ ) did not allow a full decomposition of  $\text{Ca}_3\text{Co}_2\text{O}_6$  phase. However, the long term annealing of  $\text{Ca}_3\text{Co}_2\text{O}_6$  under the determined temperature of decomposition at 1000 K in oxygen atmosphere for 336 hours led to a formation of  $\text{Ca}_3\text{Co}_{3.93+x}\text{O}_{9+\delta}$  and  $\text{Ca}_{1-x}\text{Co}_x\text{O}$ , though the transformation was never complete. This fact was confirmed by XRD and SEM measurements, where the formation of layered misfit structure is clearly noticeable. (Figures 1 and 2).



a)



b)

Figure 1. Scanning electron micrographs (magnification 2500 $\times$ ) of  $\text{Ca}_3\text{Co}_2\text{O}_6$  - a) before long term annealing, b) after long term annealing at  $T = 1000 \text{ K}$ .

The non-stoichiometric phase  $\text{Ca}_3\text{Co}_{3.93+x}\text{O}_{9+\delta}$  exhibits a variable oxygen stoichiometry  $\delta$  depending on temperature. FactSage calculations showed that  $\delta$  indeed decreases with increasing temperature and decreasing partial pressure of oxygen. At the temperature of decomposition it reaches the value  $\delta \sim 0.226$  in air atmosphere at  $T \sim 1220 \text{ K}$ . This conforms well to the TGA experiment revealing the mass change on decomposition into  $\text{Ca}_3\text{Co}_2\text{O}_6$  and  $\text{Ca}_{1-x}\text{Co}_x\text{O}$  (with well defined oxygen content) corresponding to  $\delta \sim 0.2$ .

Moreover, as shown by our experiments the phase  $\text{Ca}_3\text{Co}_{3.93}\text{O}_{9+\delta}$  actually exhibits a narrow homogeneity range with respect to cation composition. The samples with the coefficient  $x = -0.13, -0.03, \text{ and } +0.07$  in the net formula  $\text{Ca}_3\text{Co}_{3.93+x}\text{O}_{9+\delta}$  were found single phase while those outside this homogeneity range ( $x = -0.33, -0.23, +0.17$  and  $+0.27$ ) contained the corresponding impurity phases, namely  $\text{Ca}_3\text{Co}_2\text{O}_6$  and  $\text{Co}_3\text{O}_4$  from the Ca rich and Co-rich part of the phase diagram, respectively. Let us note that nearly identical results have been reported by Zhou et al. [17]. The X-ray diffraction patterns of three samples, where  $x = -0.33, 0$  and  $+0.27$  are shown

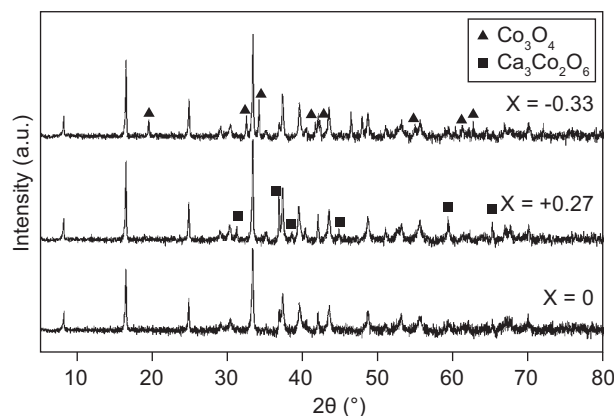


Figure 2. XRD of  $\text{Ca}_3\text{Co}_{3.93+x}\text{O}_{9+\delta}$  phase, where  $x = -0.33, 0$  and  $+0.27$ .

in Figure 2 and clearly demonstrate the presence of the pertinent impurity phases in the first and the third case compared to the phase pure  $x=0$  composition. The narrow homogeneity range of  $\text{Ca}_3\text{Co}_{3.93+x}\text{O}_{9+\delta}$  is satisfactorily reproduced by our thermodynamic calculations as shown in Figure 3. The corresponding thermodynamic model based on compound energy formalism was in detail described in [8]. In brief, since the misfit ratio remains constant over the whole homogeneity range, the departure from ideal stoichiometry is attributed, respectively, to  $\text{Ca}^{2+}$  for  $\text{Co}^{3+}$  and  $\text{Co}^{2+}$  for  $\text{Ca}^{2+}$  substitution in the case of  $x < 0$  and  $x > 0$ , both point defects being formed within the rock-salt block. According to the proposed model, the homogeneity range becomes narrowing with increasing temperature and comes to a point located in Co-rich region at peritectoid decomposition.

DTA curves of all samples measured in purified air are illustrated in Figure 4. The temperature of eutectoid transition where the  $\text{Ca}_3\text{Co}_{3.93+x}\text{O}_{9+\delta}$ – $\text{Co}_3\text{O}_4$  mixture transforms into Co-rich  $\text{Ca}_{1-x}\text{Co}_x\text{O}$  solution of rock-salt type was experimentally determined at  $\sim 1170$  K in air atmosphere (for  $x_{\text{Co}} \sim 0.98$ ).  $\text{Ca}_3\text{Co}_{3.93+x}\text{O}_{9+\delta}$  is thermodynamically stable up to  $\sim 1220$  K where it undergoes a peritectoid decomposition into  $\text{Ca}_3\text{Co}_2\text{O}_6$  and  $\text{Co}_{1-x}\text{Ca}_x\text{O}$ . Moreover, as identified on the measured heat capacity curve (Figure 5) there are two peaks

Table 1. Comparison of experimental and calculated data of phase transformations for  $p_{\text{O}_2}/p^0 = 0.21$  ( $p^0 = 101.3$  kPa).

	$\text{Ca}_3\text{Co}_{3.93}\text{O}_{9+\delta} + \text{Co}_3\text{O}_4 \leftrightarrow \text{Co}_{1-x}\text{Ca}_x\text{O}$	
	DSC	FactSage
$T$ (K)	$1169 \pm 5$	1167.55
	$\text{Ca}_3\text{Co}_{3.93}\text{O}_{9+\delta} \leftrightarrow \text{Ca}_3\text{Co}_2\text{O}_6 + \text{Co}_{1-x}\text{Ca}_x\text{O}$	
	DSC	FactSage
$T$ (K)	$1222 \pm 13.44$	1210.72

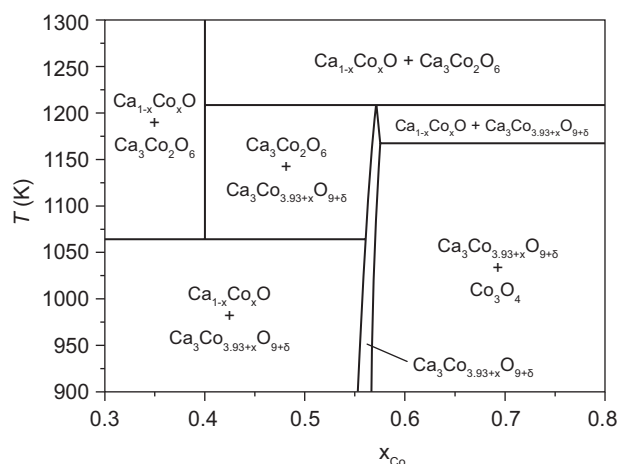


Figure 3. Phase diagram section of Ca–Co–O system in air atmosphere ( $p_{\text{O}_2}/p^0 = 0.21$ , where  $p^0 = 101.3$  kPa).

centered at  $\sim 400$  K and at  $\sim 840$  K whose origin is discussed hereinafter.  $\text{Ca}_3\text{Co}_2\text{O}_6$  is stable from  $\sim 990$  K up to  $\sim 1310$  K, at higher temperatures it decomposes into Ca-rich and Co-rich  $\text{Co}_{1-x}\text{Ca}_x\text{O}$  revealing a large miscibility gap. Experimental and calculated data of phase transformations are compared in Table 1. Based on these results and on *FactSage* calculations a relevant part of Ca–Co–O phase diagram involving both ternary oxides,  $\text{Ca}_3\text{Co}_{3.93+x}\text{O}_{9+\delta}$  and  $\text{Ca}_3\text{Co}_2\text{O}_6$ , was constructed for  $p_{\text{O}_2}/p^0 = 0.21$  ( $p^0 = 101.3$  kPa) (Figure 3).

A close inspection of heat capacity curve at low temperatures reveals two effects at  $T_F \sim 15$  K and  $T_{SDW} \sim 22$  K which have been identified with a ferrimagnetic ordering of Co in  $[\text{Ca}_2\text{CoO}_3]$  blocks and a spin density wave formation in  $[\text{CoO}_2]$  blocks, respectively [13].

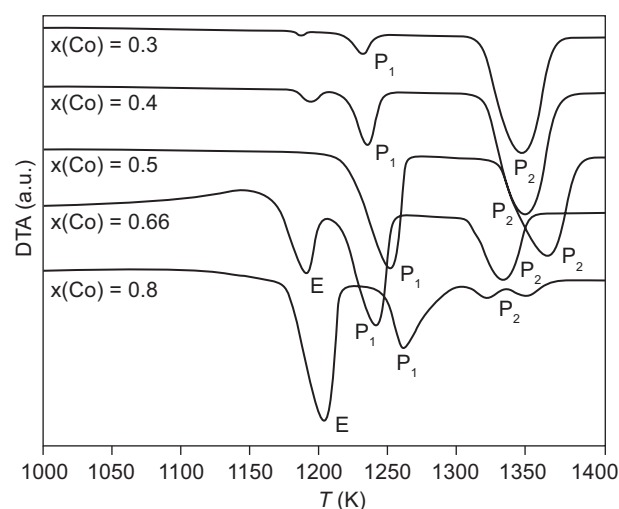


Figure 4. DTA curves of measured samples in purified air atmosphere ( $p_{\text{O}_2}/p^0 = 0.21$ , where  $p^0 = 101.3$  kPa). E is eutectoid transition,  $P_1$  is peritectoid decomposition of  $\text{Ca}_3\text{Co}_{3.93+x}\text{O}_{9+\delta}$  and  $P_2$  is peritectoid decomposition of  $\text{Ca}_3\text{Co}_2\text{O}_6$ .

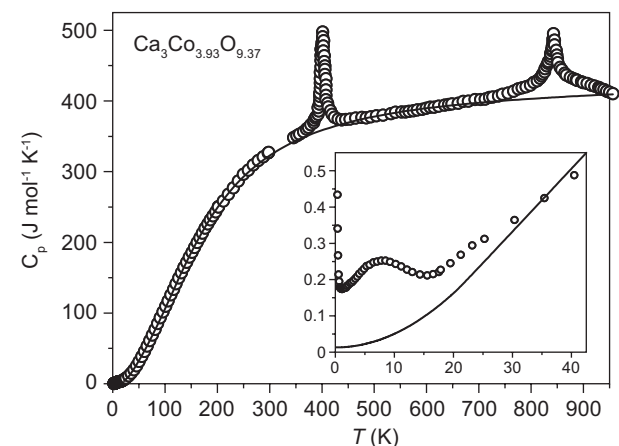


Figure 5. Heat capacity of  $\text{Ca}_3\text{Co}_{3.93}\text{O}_{9+\delta}$ . Experimental data measured by PPMS and DSC (open symbols), calculated according to Debye–Einstein and Sommerfeld model (solid line). Inset –  $C_p/T$  vs.  $T$  below 40 K manifesting the magnetic excitations.

Moreover, the analysis of  $C_p$  below 1 K, where both the lattice and magnetic excitations are suppressed, provided the value of electronic specific heat term  $\gamma \sim 50 \text{ mJ}\cdot\text{mol}^{-1}\cdot\text{K}^{-2}$  [13]. However, if we applied this value on analyzing the heat capacity at elevated temperatures by considering both the electronic and phonon contribution, we never succeeded to reproduce the experimental data above room temperature (the theoretical curve always exceeded the experimental one). We thus considered the Sommerfeld coefficient  $\gamma$  specifying the electronic part of heat capacity

$$C_{el} = \gamma T \quad (3)$$

as a parameter which was fitted together with the other parameters representing the lattice contribution to heat capacity. The obtained value  $\gamma = 13.2 \pm 1.0$  suggests that there must be a renormalization of density of states at Fermi level  $N(E_F)$  upon crossing the magnetic transitions at low temperatures resulting in substantially lower value of  $\gamma = \mathbf{R}(2\pi^2/3)N(E_F)k_B T$ , indeed on the assumption that our  $C_p$  data above room temperature are correct.

The analysis of the lattice heat capacity was based on an additive combination of Debye and Einstein models. The phonon spectrum of a polyatomic compound contains three acoustic branches and  $3n - 3$  optical ones, where  $n$  is number of atoms per primitive unit cell. In our case, considering the structure formula  $[\text{Ca}_2\text{CoO}_3][\text{CoO}_2]_{1.62}$ , this represents 29.58 optical branches. The acoustic part of the phonon specific heat is then described using the Debye model in the form

$$C_{\text{phD}} = 9\mathbf{R} \left( \frac{T}{\Theta_D} \right)^3 \int_0^{x_D} \frac{x^4 \exp(x)}{(\exp(x) - 1)^2} dx \quad (4)$$

where  $\mathbf{R}$  is the gas constant,  $\Theta_D$  is the Debye characteristic temperature and  $x_D = \Theta_D/T$ . Here the three acoustic branches are taken as one triply degenerate branch, which was attributed to the rock-salt block. Although this choice is rather arbitrary, it is partly substantiated by the fact that  $[\text{CoO}_2]$  blocks are more rigid and their atoms are thus supposed to predominantly contribute to high frequency phonon modes. Similarly, the individual optical branches are described by the Einstein model

$$C_{\text{phEi}} = \mathbf{R} \cdot \frac{w_i x_{Ei}^2 e^{x_{Ei}}}{(e^{x_{Ei}} - 1)^2} \quad (5)$$

where  $x_{Ei}$  has an analogous meanings as in the previous case and  $w_i$  refers to a degeneracy of the corresponding Einstein mode. The heat capacity then reads

$$C_p = C_{el} + \frac{3}{2} \left( C_{\text{phD}} + \sum_{i=1}^3 C_{\text{phEi}} \right) \quad (6)$$

where the sum runs over three Einstein modes whose degeneracies are specified in Table 2 and the factor 3/2 is applied to renormalize the resulting lattice heat capacity from the structure formula  $[\text{Ca}_2\text{CoO}_3][\text{CoO}_2]_{1.62}$  to the net formula  $\text{Ca}_3\text{Co}_{3.93}\text{O}_{9.36}$ . Let us note that the grouping of several optical phonon modes into a single Einstein mode with a degeneracy  $w_i$  is again arbitrary and is only

qualified by the requirement of reasonable number of free parameters and the best achievable fit to experimental data. The first two Einstein modes apparently correspond to rock-salt block while the last one (with a non-integer  $w_i$ ) to  $[\text{CoO}_2]$  layer. Interestingly, the fitting procedure was originally started with two different modes per  $[\text{CoO}_2]$ , however, the resulting parameters were quite close to each other and highly interdependent, so they were grouped into a single mode in the next step. The model parameters given in Table 2 and the resulting fitting curve shown in Figure 5 are based on a non-linear least-square fit applied on the measured heat capacity data from the temperature ranges 30 – 298 K and 490 – 650 K where the heat capacity is supposed to involve only the terms specified in Eq.(6).

Table 2. Parameters of Debye-Einstein model for lattice heat capacity ( $\Theta_D$  and  $\Theta_{Ei}$ ) evaluated by non-linear least-square fit.

	D	E <sub>1</sub>	E <sub>2</sub>	E <sub>3</sub>
$\Theta_D/\text{K}$	$198 \pm 14$	$241 \pm 13$	$480 \pm 14$	$678 \pm 10$
$w_i$	3	5	10	14.58

The absolute entropy of  $\text{Ca}_3\text{Co}_{3.93+x}\text{O}_{9+\delta}$  at the reference temperature  $T = 298.15 \text{ K}$  was evaluated by integrating the experimental data of heat capacity divided by the thermodynamic temperature from lowest available temperature  $T = 0.35 \text{ K}$  up to ambient temperature. The obtained value  $S_{298}^\circ = 297.3 \text{ J}\cdot\text{mol}^{-1}\cdot\text{K}^{-1}$  involves the phonon part ( $289.5 \text{ J}\cdot\text{mol}^{-1}\cdot\text{K}^{-1}$ ) calculated from Debye-Einstein model and electronic part ( $3.9 \text{ J}\cdot\text{mol}^{-1}\cdot\text{K}^{-1}$ ) approximated by Sommerfeld model. The remainder ( $3.9 \text{ J}\cdot\text{mol}^{-1}\cdot\text{K}^{-1}$ ) consists predominantly of magnetic entropy (FM and SDW) and Schottky-type contribution from the effect of cobalt hyperfine field at very low temperatures. These low temperature excitations are in detail depicted in the inset of Figure 5. The second principal thermodynamic quantity, enthalpy of formation from elements,  $\Delta_f H_{298}^\circ = -3206 \text{ kJ}\cdot\text{mol}^{-1}$ , was derived from equilibrium condition for the peritectoid decomposition of  $\text{Ca}_3\text{Co}_{3.93}\text{O}_{9+\delta}$  into  $\text{Ca}_3\text{Co}_2\text{O}_6 + \text{Co}_{1-x}\text{Ca}_x\text{O}$  using the measured heat capacity and third-law value of entropy for  $\text{Ca}_3\text{Co}_{3.93}\text{O}_{9+\delta}$ , as well as the relevant data for  $\text{Ca}_3\text{Co}_2\text{O}_6$  and  $\text{Co}_{1-x}\text{Ca}_x\text{O}$  evaluated in the previous step ( $\Delta_f H_{298}^\circ$  of  $\text{Ca}_3\text{Co}_2\text{O}_6$  was determined in a similar way from its decomposition into Co-rich and Ca-rich  $\text{Co}_{1-x}\text{Ca}_x\text{O}$  solid solution).

The analysis of phonon and electronic part of heat capacity made it possible to separate both peaks detected on the measured heat capacity curve above ambient temperature and to evaluate the corresponding enthalpy and entropy changes (see Table 3). The first effect centered at  $T_{T1} = 400 \text{ K}$  can be unambiguously attributed to oxygen ordering in the central  $[\text{CoO}]$  layer of the rock-salt block which has been recently studied by Muguerra et al [18-19]. They found that above the transition temperature the structural pattern of the  $[\text{CoO}]$  layer is built of triple

–{Co<sub>3</sub>O<sub>3</sub>}– chains whereas below this temperature a cooperative atomic displacements of oxygen atoms yields {CoO<sub>2</sub>} and {Co<sub>5</sub>O<sub>4</sub>} clusters. If we take into account the coordinating oxygen atoms in adjacent [CaO] layers then cobalt is square-planar coordinated in {CoO<sub>2</sub>} while {Co<sub>5</sub>O<sub>4</sub>} clusters consist of four tetrahedra and one central octahedron. While the tetrahedral coordination of Co at the triple chain edges is roughly preserved on crossing the transition, the cobalt sitting at the central average position (octahedral coordination) above the transition is split by displacements of surrounding oxygen atoms in two new positions – square planar and compressed octahedron. Hence the corresponding entropy change should correspond to  $\Delta S_{T_1} = 3/2 R \ln 2 = 8.64 \text{ J}\cdot\text{mol}^{-1}\cdot\text{K}^{-1}$ , which is in satisfactory agreement with our experimental value. Let us note that the particular mechanism of such cooperative atomic displacement is based on „softening“ of particular phonon modes ending eventually in freezing of the respective atoms at new positions and the corresponding symmetry lowering. As phonons are involved in the whole process and their energy, degeneracy and in turn the specific features of the phonon spectrum are altered, the simple Debye-Einstein model seems to be apparently a crude approximation when used for background subtraction in this case.

Unlike the first transition which is undoubtedly of structural origin, the second effect centered at  $T_{T_2} = 840 \text{ K}$  is not accompanied by any noticeable structural change as documented by high temperature XRD and neutron diffraction experiments performed on our samples. Yet both effects must be interrelated since none of them has been detected on a sample prepared at more reducing conditions and thus exhibiting a lowered oxygen content [13]. Based on the analysis of magnetic susceptibility data indicating an intermediate spin (IS,  $S_{IS} = 1$ ) of Co<sup>3+</sup> in rock-salt block in a broad temperature range (20–380 K), we believe that this effect is connected to a spin transition of this cobalt cation from IS state to high spin state (HS,  $S_{HS} = 2$ ). The entropy change associated with this transition can be expressed as  $\Delta S_{T_2} = (3/2) R \ln((2S_{HS}+1)/(2S_{IS}+1)) = (3/2) R \ln(5/3) = 6.37 \text{ J}\cdot\text{mol}^{-1}\cdot\text{K}^{-1}$ , which fits the experimental value in Table 3 remarkably well.

Table 3. Temperatures  $T_{T_i}$ , enthalpy changes  $\Delta H_{T_i}$ , and entropy changes  $\Delta S_{T_i}$  corresponding to transitions  $T_1$  and  $T_2$  identified as two peaks on the heat capacity of Ca<sub>3</sub>Co<sub>3.93</sub>O<sub>9+δ</sub>. The temperatures are referred to peak maxima.

	$T_{T_i}/\text{K}$	$\Delta H_{T_i}/\text{J mol}^{-1}$	$\Delta S_{T_i}/\text{J}\cdot\text{K}^{-1}\cdot\text{mol}^{-1}$
$T_1$	400	3040	8.01
$T_2$	842	5510	6.67

## CONCLUSION

The misfit layer cobaltite Ca<sub>3</sub>Co<sub>3.93+x</sub>O<sub>9+δ</sub> reveals a narrow homogeneity range from  $x = -0.13$  to  $x = +0.07$

and a variable oxygen content  $\delta$ . Depending on oxygen activity in the surrounding atmosphere it undergoes a peritectoid decomposition into Ca<sub>3</sub>Co<sub>2</sub>O<sub>6</sub> and Co<sub>1-x</sub>Ca<sub>x</sub>O solid solution. This behavior has been experimentally observed and thermodynamically modeled in terms of compound energy formalism and the corresponding  $x_{\text{Co}}-T-p_{\text{O}_2}$  phase diagram was constructed. The input thermodynamic data were assessed from the high temperature equilibrium data and from heat capacity measurements performed in broad temperature range. The heat capacity data were analyzed in terms of Debye-Einstein model for lattice heat capacity and Sommerfeld electronic specific heat term. The excess terms manifested in particular as two distinct peaks on the heat capacity curve centered at 400 and 840 K were interpreted as displacive arrangement of oxygen atoms and spin state transition, both occurring within the central [CoO] layer of the [Ca<sub>2</sub>CoO] rock-salt block.

## References

- Miyazaki Y.: *Solid State Ion.* 172, 463 (2004).
- Lambert S., Leligny H., Grebille D.: *J. Solid State Chem.* 160, 322 (2001).
- Xua L., Li F., Wang Y.: *J. Alloy Compd.* 501, 115 (2010).
- Wang D., Chen L., Yao Q., Li J.: *Solid State Commun.* 129, 615 (2004).
- Wang D., Chen L., Wang Q., Li J.: *J. Alloy Compd.* 376, 58 (2004).
- Liu H.Q., Zhao X.B., Zhu T.J., Song Y., Wang F.P.: *Curr. Appl. Phys.* 9, 409 (2009).
- Shimoyama J., Horii S., Otschi K., Sano M., Kishio K.: *Jpn.J.Appl.Phys.* 42, L194 (2003).
- Sedmidubsky D., Jakes V., Jankovsky O., Leitner J., Sofer Z., Hejtmanek J.: Phase Equilibria in Ca-Co-O System, to appear in *J. Solid. State. Chem.* DOI: 10.1016/j.jssc.2012.05.014 (2012).
- Kenfaui D., Chateigner D., Gomina M., Noudem J. G.: *J. Alloys Compd.* 490, 472 (2010).
- Leitner J., Sedmidubsky D., Ruzicka K., Svoboda P.: *Thermochim Acta* 531, 60 (2012).
- Hardy V., Lees M., Maignan A., H'ebert S., Flahaut D., Martin C., Paul M., *J. Phys.:Condens. Matter* 15, 5737 (2003).
- I.-H Jung, Deckerov S., Pelton A., Kim H.-M., Kang Y.-B.: *Acta Materialia* 52, 507 (2004).
- Hejtmanek J., Knizek K., Marysko M., Jirak Z., Sedmidubsky D., Jankovsky O., Huber S., Masschelein P., Lenoir B.: *J. Appl. Phys.* 111, 07D715 (2012).
- Jacob K., Shekhar C., Kale G.: *J. Phase Equilib. Diffusion* 30, 2 (2009).
- Woermann E., Muan A.: *J. Inorg. Nucl. Chem.* 32, 1455 (1970).
- Chen M., Hallstedt B., Gauckler L.: *J. Phase Equilib.* 24, 212 (2003).
- Zhou X.-D., Pederson L., Thomsen E., Nie Z., Coffey G.: *J. Electrochemical and Solid State Letters* 12, F1–F3 (2009).
- Muguerra H., Grebille D., Bourée F.: *Acta Cryst. B* 64, 144 (2008).
- Muguerra H., Grebille D.: *Acta Cryst. B* 64, 767 (2008).